ChemPhysChem

Research Article
doi.org/10.1002/cphc.202200787

Chemistry Europe
European Chemical Societies Publishing

www.chemphyschem.org

Interaction of CO_2 with MnO_x/Pd(111) Reverse Model Catalytic Interfaces

Arca Anil,[a] Omer Faruk Sadak,[a] Bartu Karakurt,[a] Yusuf Kocak,[a] Igor Lyubinetsky,*[a] and Emrah Ozensoy*[a, b]

Understanding the activation of CO_2 on the surface of the heterogeneous catalysts comprised of metal/metal oxide interfaces is of critical importance since it is not only a prerequisite for converting CO_2 to value-added chemicals but also often, a rate-limiting step. In this context, our current work focuses on the interaction of CO_2 with heterogeneous bi-component model catalysts consisting of small MnO_x clusters supported on the Pd(111) single crystal surface. These metal oxide-on-metal 'reverse' model catalyst architectures were investigated via temperature programmed desorption (TPD) and x-ray photoelectron spectroscopy (XPS) techniques under ultra-high vacuum (UHV) conditions. Enhancement of CO_2 activation was observed upon decreasing the size of MnO_x nanoclusters by lowering the preparation temperature of the catalyst down to 85 K. Neither pristine Pd(111) single crystal surface nor thick (multilayer) MnO_x overlayers on Pd(111) were not capable of activating CO_2, while CO_2 activation was detected at sub-monolayer (~0.7 ML) MnO_x coverages on Pd(111), in correlation with the interfacial character of the active sites, involving both MnO_x and adjacent Pd atoms.

Introduction

Mitigating the negative impact of anthropogenic atmospheric carbon emissions on climate change continues to increase its importance. Hence, the conversion of carbon dioxide and fossil fuel combustion products in the atmosphere to fuels or other industrially useful value-added hydrocarbon compounds is an attractive approach for CO_2 utilization.[1–8] Hydrogenation of CO_2 is a challenging process due to the difficulties associated with the activation of CO_2, a thermodynamically very stable molecule.[9–11] Achieving energy-efficient CO_2 conversion to fuels requires development of innovative catalytic approaches and new catalysts. In particular, heterogeneous catalytic strategies utilizing proper combinations of metal and metal oxide components with complementary chemical properties often facilitates the reaction pathways for CO_2 hydrogenation.[7–8] The combination of the acid-base sites of metal oxides with the active metal sites is a commonly exploited catalytic strategy to facilitate CO_2 reduction by hydrogen.[12–13] Bi-component catalysts consisting of late-transition metal nanoparticles (e.g., Rh, Cu, and Ni) on metal oxide supports (e.g., ZnO, SiO_2, and ZrO_2) have been shown to be active in the reduction of CO_2 to fuels (e.g., methanol and methane) or other valuable chemical feedstocks (e.g., formic acid).[14–19] Although some understanding of cause-and-effect relationships for these types of catalysts have been advanced, in particular, for Cu/ZnO,[17–19] sufficient control over CO_2 reduction has not been achieved to obtain a truly efficient catalytic process.

In order to design new catalytic architectures for CO_2 activation, new types of metal/metal-oxide interfaces should be explored, where the properties of both metal and the metal oxide phases have to be optimized. Particularly, such optimization efforts may involve the control of the size, shape, and dispersion of the metal particles,[20] along with adjustments of chemical state, composition, and morphology of the oxide domains.[21–23] In the majority of the former heterogeneous catalytic studies associated with the metal-oxide systems, the catalyst of interest typically contains metal particles dispersed on the oxide support. However, a relatively little attention has so far been devoted to the so called 'reverse' model catalyst systems, consisting of the oxide particles supported on an atomically well-defined planar single crystal metal substrate.[24–25] Similar to metal-on-oxide catalysts,[26–28] the activity and selectivity of oxide-on-metal catalysts could also be affected by the size of the oxide particles, the interactions between the oxide and the metal support, and the charge transfer between them. Manganese oxide nanoparticles on a palladium single crystal support can be considered as an appropriate bi-component 'reverse' model catalyst. While Pd is not known to promote CO_2 activation,[29–30] it can efficiently activate H_2 via dissociation of molecular hydrogen.[31–34] On the other hand, it has been recently reported that MnO_x–based catalysts could readily facilitate CO_2 hydrogenation to C_{5+} hydrocarbons.[35] Note also that Mn is the third most abundant transition metal and has much lower toxicity than many other metals used in CO_2 hydrogenation.[36] Among several stable manganese oxide phases, manganese (II) oxide (MnO) is

[a] A. Anil, O. F. Sadak, B. Karakurt, Dr. Y. Kocak, Dr. I. Lyubinetsky, Prof. Dr. E. Ozensoy
Department of Chemistry, Bilkent University, 06800 Ankara, Turkey
E-mail: igor@bilkent.edu.tr
ozensoy@fen.bilkent.edu.tr
[b] Prof. Dr. E. Ozensoy
UNAM – National Nanotechnology Research Center, Institute of Materials Science and Nanotechnology, Bilkent University, 06800 Ankara, Turkey

Supporting information for this article is available on the WWW under https://doi.org/10.1002/cphc.202200787

commonly observed at low oxygen partial pressures.[37] Because of the large lattice mismatch (>10%) between the bulk crystal structure of MnO and the Pd(111) substrate,[25] aggregation of MnO clusters and discrete MnO nanoparticle formation are expected rather than the growth of continuous MnO overlayers. However, not much is known about CO_2 interaction on Mn oxides.[38]

An effective binding and activation of CO_2 on the catalyst surface are the very initial steps of CO_2 conversion to fuels. Hence, in the current article, we report our findings on $^{13}CO_2$ adsorption and activation on bi-component 'reverse' model catalysts in oxide-on-metal configuration, consisting of small MnO_x clusters deposited on the Pd(111) support surface. Using temperature programed desorption (TPD) and x-ray photoelectron spectroscopy (XPS), we focus on the $^{13}CO_2$ uptake characteristics, and the variation of different $^{13}CO_2$ desorption states as a function of i) MnO_x overlayer coverage, ii) Mn oxidation state, iii) the chemical nature/morphology of the active sites on the model catalysts prepared at room temperature (RT) vs. low temperature (85 K).

Results and Discussion

TPD profiles for the m/z=45 desorption channel shown in Figure 1 were obtained by a gradual increase of $^{13}CO_2$ exposure at 85 K over a 1.5 monolayer (ML) MnO_x overlayer grown on Pd(111) at RT. As illustrated in Figure S1, 15 L $^{13}CO_2$ adsorption experiments at 85 K for different MnO_x overlayer coverages within 0.7–6 ML display similar desorption features to the corresponding high exposure $^{13}CO_2$ data given in Figure 1. In Figure 1, the principal desorption peak (α_2) is detected at ~105 K, indicating a rather weak interaction between $^{13}CO_2$ and the surface corresponding to a physisorbed CO_2 state. A single TPD peak is visible for $^{13}CO_2$ exposures <0.3 L at 110 K, while the formation of a low temperature shoulder at ~90 K is observed for higher exposures (≥0.3 L). Increasing the $^{13}CO_2$ exposure above 0.3 L leads to the simultaneous growth of both of these aforementioned features and the eventual saturation of the α_2 state. Notably, the evolution of the α_2 peak closely resembles that of $^{13}CO_2$ desorption from the *clean* Pd(111) surface, as can be seen in Figure S2. Hence, α_2 desorption peak is predominantly associated with $^{13}CO_2$ adsorption on the Pd sites of the MnO_x(1.5 ML)/Pd(111) surface. On the other hand, the low temperature shoulder at ~90 K which partially overlaps with the α_2 peak can be attributed to an extremely weakly bound multilayer $^{13}CO_2$ adsorption state, whose desorption temperature is lower than the lowest temperature attainable in the currently used UHV setup (i.e., 85 K). Hence, this multilayer desorption peak at T<85 K cannot be fully monitored in the current TPD plots. In comparison with the pristine Pd(111) (Figure S2), the presence of ultra-thin MnO_x overlayers grown at RT (Figure 1) causes relatively minor but detectable modifications of the $^{13}CO_2$ TPD profiles. Figure 1 shows that on the MnO_x(1.5 ML)/Pd(111) surface, a shoulder feature (i.e., α_1) starts to appear on the high temperature tail of the α_2 desorption peak at high $^{13}CO_2$ exposures, along with an additional weak feature (i.e., β_1) at ~330 K. As the α_1 feature does not exist for the pristine Pd(111) surface (Figure S2), development of the α_1 peak on the MnO_x(1.5 ML)/Pd(111) surface apparently indicates the population of new MnO_x–associated physisorbed $^{13}CO_2$ states with slightly higher adsorption energies as compared to that of α_2. On the other hand, high desorption temperature of the β_1 feature corresponds to a strong bonding between $^{13}CO_2$ and MnO_x sites, and could be provisionally attributed to CO_2 activation. In contrast to a physisorbed form of $^{13}CO_2$ (with a linear geometry) associated with α_2 and α_1 peaks, β_1 peak could be related to a chemisorbed form of $^{13}CO_2$ with a bent conformation, which is stabilized by a partial negative charge induced by electron capture (i.e., $CO_2^{\delta-}$). Note that, similar $CO_2^{\delta-}$ species were also reported in former studies investigating CO_2 adsorption on late-transition metals such as Cu(111)).[12,39]

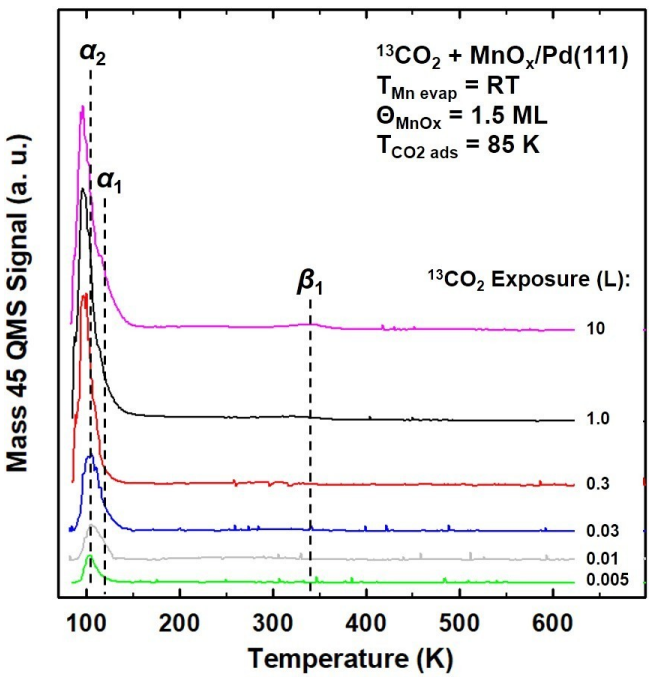

Figure 1. m/z=45 TPD profiles upon increasing $^{13}CO_2$ exposure over MnO_x-(1.5 ML)/Pd(111) surface prepared at room temperature.

It is well-known that catalytic activity and/or selectivity of metal oxide clusters may critically depend on their relative particle size.[40–45] Since MnO_x cluster size on the Pd(111) support could be controlled by the Mn deposition temperature, we modified the currently investigated model catalyst structure by forming MnO_x at a distinctively lower temperature of 85 K, which ought to considerably decrease the size of clusters and potentially enhance CO_2 activation. Importantly, the temperature of 85 K is low enough to eliminate the aggregation of small clusters into larger ones via surface diffusion, as it is well within the Zone 1 of Sanders classification (defined by $T/T_m < 0.1$, T_m is the melting point of Mn and/or MnO),[46] where the surface diffusion is hindered and the growth is dominated by the simple shadowing process (i.e., the angular directions of the incident coating atoms are governed by the simple geometric interaction due to the roughness of the growing

surface). As a result, incoming atoms should largely reside in their condensation positions, and at initial stages of growth, majority of them should remain as clusters with sub-nanometer diameters and, in the extreme case, may exist as monomers. As deposition continues, the random sticking of atoms in upper layers and resulting atomic stacking and shadowing effects increase the surface roughness and yield a dense packing.[46–47]

Figure 2 presents typical m/z = 45 TPD profiles for increasing $^{13}CO_2$ exposures over MnO_x(1.5 ML)/Pd(111) surface prepared at 85 K. As a key difference in comparison with the adsorption over MnO_x(1.5 ML)/Pd(111) formed at RT (Figure 1), in Figure 2, even at very low $^{13}CO_2$ exposures, a fairly intense β_1 peak gradually grows without the formation of any α_1 or α_2 states. (As a side remark, note that the origin of the β_1 peak shift from ~350 K to ~370 K with increasing $^{13}CO_2$ exposure is currently unclear). Figure 2 also indicates that while strongly bound β_1 state is populated first, two distinct α_1 and α_2 TPD peaks emerge simultaneously upon further $^{13}CO_2$ exposure (> 0.02 L).

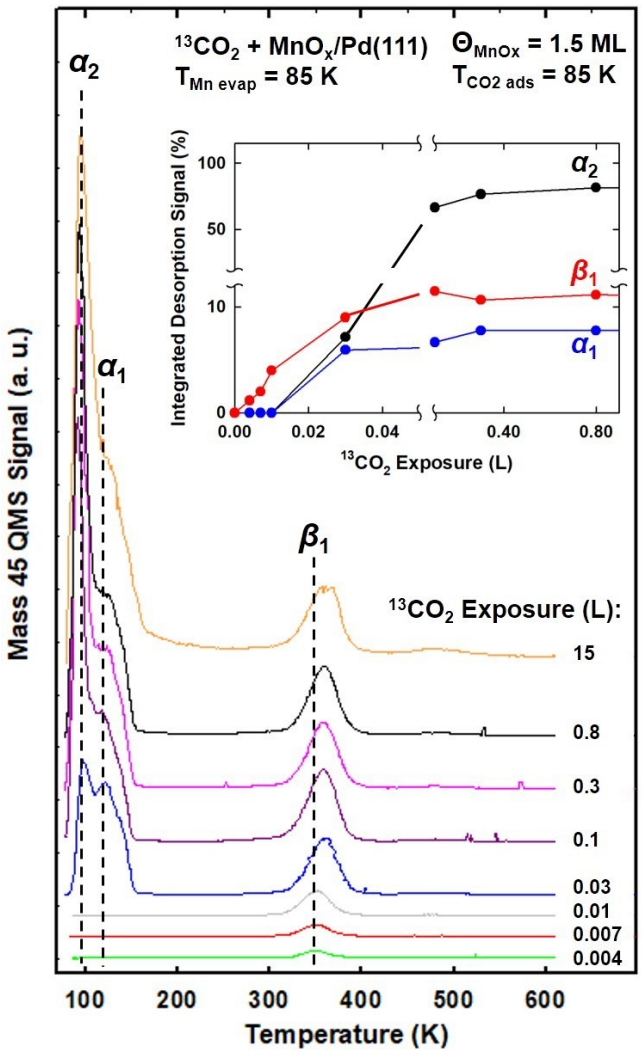

Figure 2. m/z = 45 TPD profiles upon increasing $^{13}CO_2$ exposure over MnO_x (1.5 ML)/Pd(111) surface prepared at 85 K. Inset shows the variation of the relative integrated TPD signals of α_1, α_2, and β_1 desorption states as a function of $^{13}CO_2$ exposure.

As mentioned earlier, relatively low desorption maxima of α_1 (120 K) and α_2 (100 K), are consistent with the presence of physisorption states. While α_2 peak is largely associated with the first $^{13}CO_2$ sub-monolayer weakly-bound on Pd(111),[48] α_1 peak possibly corresponds to a desorption from MnO_x and/or interfacial MnO_x–Pd sites, where $^{13}CO_2$ is bonded only slightly stronger than that of α_2 state. Inset of Figure 2 shows normalized m/z = 45 desorption yields from different adsorption states as a function of $^{13}CO_2$ exposure. The β_1 state which can be associated with an activated $^{13}CO_2$ species, virtually saturates at ε ~0.03 L. It is apparent that while the desorption intensities of α_1 and β_1 states, which are associated with MnO_x clusters, quickly saturate at relatively lower $^{13}CO_2$ exposures of ca. 0.03 L, α_2 desorption state due to Pd(111) sites continue to grow in intensity up to a $^{13}CO_2$ exposure of ca. 0.10 L.

We suggest that β_1 TPD peak observed in Figure 2 could be linked to an activated CO_2 preferentially chemisorbed on MnO_x to form charged $CO_2^{\delta-}$ (carboxylate-like) and/or CO_3^{2-} (carbonate) surface complexes, as reported elsewhere for various metal/metal oxide catalysts.[35,49–53] This argument is also in line with the former infrared spectroscopic data obtained upon chemisorption of CO_2 on the Co/MnO_x catalyst, where charged $CO_2^{\delta-}$ species have been identified.[35] Remarkably, one of the prominent features in the CO_2 TPD profile of the on Co/MnO_x catalyst has been a desorption signal at 364 K,[35] whose temperature is in close proximity to that of the β_1 peak (~370 K) in the current work (Figure 2). Furthermore, similar CO_2 TPD peaks within 353–365 K have also been reported for both Cu/ZnO and reduced $LaCrO_3$ catalysts,[49–50] and the corresponding infrared spectra have revealed both monodentate and bidentate carbonates.[49–50] Also note that for methanol synthesis catalysts, a reaction mechanism has been suggested, where the formation of a transient carbonate intermediate is invoked as the key and perhaps the rate-limiting step.[51–53] However, as the exact nature of the intermediate species observed in this work is currently undetermined, additional direct spectroscopic studies are necessary.

In order to comprehend the marked difference in CO_2 activation for MnO_x clusters formed on Pd(111) at room temperature vs. low temperature, we examined the differences in their Mn oxidation states. Figure 3a shows Mn $3p_{3/2}$ XPS spectrum along with deconvoluted XPS signals corresponding to various Mn oxidation states of MnO_x(1.5 ML)/Pd(111) prepared at RT. As has been discussed in one of our recent reports,[54] similar to Mn-containing compounds and surface alloys, for ultra-thin (~1 ML) Mn films deposited on d-metal surfaces such as Pd,[55] Mn $2p_{3/2}$ peak attributed to Mn^0 shifts to a higher binding energy (~640 eV) in comparison with bulk Mn, and also has an intense 'shake-up' satellite separated by ~5 eV.[56–58] Moreover, the main Mn^0 XPS peak exhibits an additional 'shoulder' located below 640 eV.[55,57] All these Mn^0–associated features could be seen in the XPS spectrum in Figure 3a. On the other hand, the peak located at 642.4 eV, along with a strong 'shake-up' satellite separated by ~6 eV, is assigned to the Mn^{2+} species,[59–61] whereas the peak located at 643.6 eV is attributed to the presence of Mn^{3+} species.[62–64] Overall, the XPS data in Figure 3a show that while MnO_x clusters

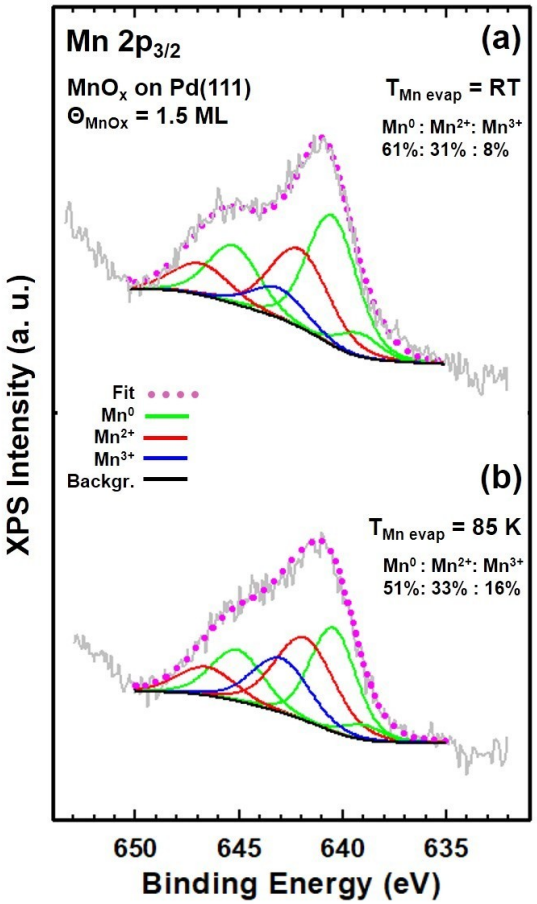

Figure 3. Mn $3p_{3/2}$ XPS spectra for the MnO_x(1.5 ML)/Pd(111) surface prepared at (a) RT and (b) 85 K.

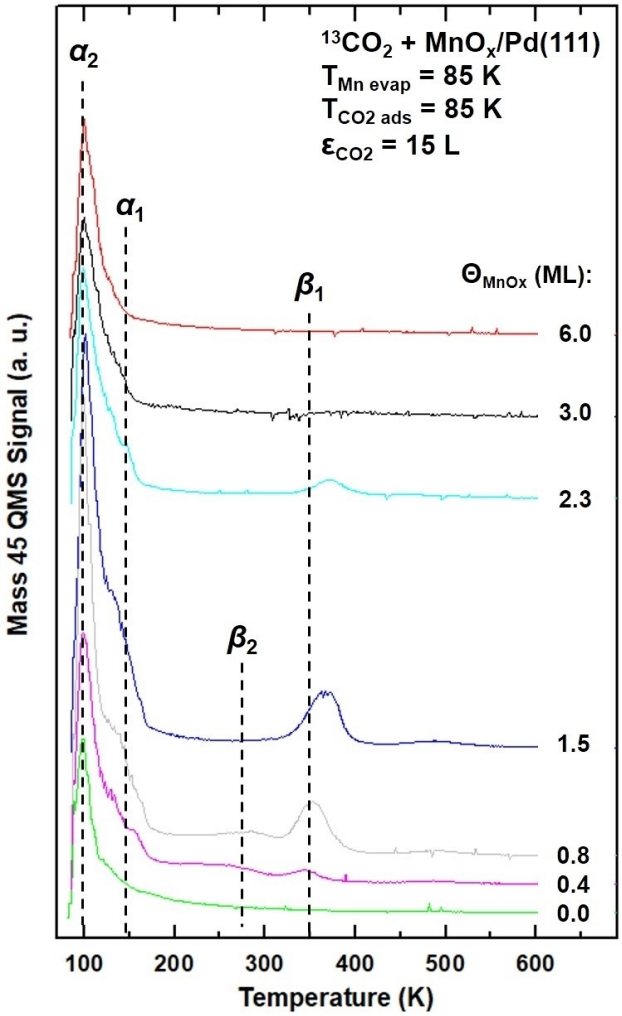

Figure 4. m/z = 45 TPD profiles upon saturation $^{13}CO_2$ exposure of MnO_x/Pd(111) for increasing MnO_x coverages of MnO_x formed on Pd(111) at 85 K.

formed at RT are partially oxidized, they also have a considerable metallic character (Mn^0%:Mn^{2+}%:Mn^{3+}% = 61%:31%:8%). On the other hand, Mn $3p_{3/2}$ XPS spectrum for the MnO_x(1.5 ML)/Pd(111) prepared at 85 K (Figure 3b) reveals a somewhat more oxidic character, with a particular increase in the XPS intensity of the Mn^{3+} state (Mn^0%:Mn^{2+}%:Mn^{3+}% = 51%:33%:16%). In order to test the potential role of the chemical state, we also additionally oxidized the MnO_x clusters on the MnO_x(1.5 ML)/Pd(111) surface prepared at RT (by exposing them to $\sim 2\times10^3$ L of O_2 at RT). The relevant Mn $3p_{3/2}$ XPS spectrum, shown in Figure S3, indicates a decrease in the metallic character (to 56% Mn^0). However, corresponding CO_2 TPD results, presented in Figure S4, show no enhancement of CO_2 activation. This observation indicates that rather than a trivial dependence on the relative abundances of different Mn oxidation states, CO_2 activation has a stronger dependence on the MnO_x coverage and MnO_x particle size.

Finally, we investigated the coverage effect of MnO_x clusters on the carbon dioxide activation, at the $^{13}CO_2$ saturation exposure. Figure 4 displays m/z = 45 TPD profiles upon $^{13}CO_2$ adsorption on the MnO_x(0–6.0 ML)/Pd(111) surfaces prepared at 85 K. Except for the α_2-desorption state, all other desorption states (α_1, β_1, and β_2) emerge at sub-monolayer MnO_x coverages and promptly disappear at higher MnO_x coverages (> 3 ML). The minor β_2 desorption signal located at 280 K can be tentatively assigned to an intermediate species with an adsorption energy lower than that of the β_1 state. The normalized integrated $^{13}CO_2$ TPD intensities due to the different desorption states as a function of MnO_x coverage are shown in Figure 5. Apparently, all desorption processes exhibit a maximum at relatively low MnO_x coverages (< 2 ML), whereas the highest degree of $^{13}CO_2$ activation (indicated by the maximization of the integrated intensity of the β_2 state) appears at a *sub-monolayer* MnO_x coverage of 0.8 ML. Importantly, at higher MnO_x coverages (> 2.5 ML), all desorption peaks associated with MnO_x sites (β_1, β_2 and α_1) disappear entirely. This MnO_x coverage corresponds to the complete covering of Pd sites, as evidenced by the ceasing of the dissociative adsorption of D_2 at $\Theta_{MnOx} > 2.5$ ML, as shown in Figure S5. (The dissociative adsorption of molecular hydrogen and its isotopes is well-documented on the Pd(111) surface, but does not occur on Mn and its oxides).[31–32,35] It should be mentioned that the surface completely covered by MnO_x (at $\Theta_{MnOx} \geq 3$ ML, Figure 4) exhibits

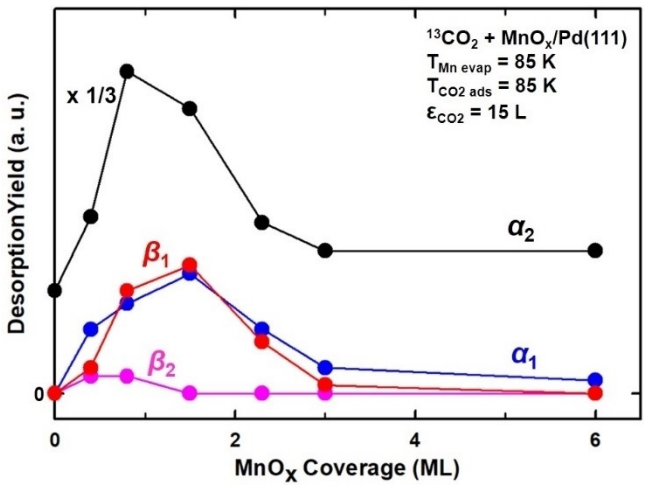

Figure 5. Normalized integrated $^{13}CO_2$ TPD intensities from different desorption states as a function of MnO_x coverage for MnO_x(0–6.0 ML)/Pd(111) surfaces prepared at 85 K. Note that α_2 curve is multiplied by $^1/_3$ for clarity.

a α_2 feature with a desorption maximum located at the same temperature (~100 K) as for clean Pd(111). This observation indicates that two separate $^{13}CO_2$ physisorption processes at both Pd and MnO_x sites, with similar adsorption energies, may contribute to the α_2 desorption channel.

An important observation of the hindering of $^{13}CO_2$ activation upon blocking of Pd sites likely points out to a necessary involvement of both MnO_x and adjacent Pd species. Apparently, these adsorption sites have an *interfacial* character (e.g., involving interface plane edges of the MnO_x nanoclusters), taking advantage of the synergy between the oxide particles and metal support.[7–8] This also well correlates with our observation of the maximum $^{13}CO_2$ activation at a relatively low MnO_x coverage (< 1 ML). While the exact nature of these active sites remains unclear, it presumably involves a strong bonding interaction between the MnO_x nanoclusters and the Pd support.[65–67] This is also in line with the B.E. shift of the Pd 3d XPS peaks towards higher values, starting from the very initial stages of Mn deposition at both RT and 85 K (Figures S6a and S6b, respectively), indicating enhanced Pd–Mn bonding, as reported by Sandell et al. for Mn on Pd(100).[55,68] Furthermore, these authors also found that at RT, Mn atoms were extensively incorporated to the subsurface layers of the Pd substrate, while such a phenomenon was absent at a lower temperature of 90 K.[68] Diffusion of Mn atoms to the Pd subsurface can attenuate the number of Mn surface atoms and decrease the available number of Pd–Mn interfacial adsorption sites on the catalyst surface leading to diminished $^{13}CO_2$ activation at RT. Another factor that can strongly influence the chemical interaction between $^{13}CO_2$ and the oxide/metal interface is the size of the MnO_x nanoparticles.[66,69] Since $^{13}CO_2$ activation is not limited solely to MnO_x/Pd(111) system formed at 85 K (minor activation was observed for RT as well, as discussed earlier), the necessity to utilize a low temperature for model catalyst preparation might be due to the increase in the number of appropriate sites via decreasing the size of oxide nanoclusters at low preparation temperatures.

Conclusions

In summary, our study demonstrates how the reactivity of oxide-on-metal interface can be fine-tuned by modifying the structure of the oxide component to generate the active sites necessary for the activation of CO_2, while alteration of the Mn oxidation states in the MnO_x does not have a significant effect on the catalytic activity. Using temperature programed desorption and x-ray photoelectron spectroscopy techniques, we examined the adsorption and activation of $^{13}CO_2$ on heterogeneous bi-component model catalyst, consisting of small MnO_x clusters supported on the Pd(111) surface. Upon decreasing the size of the MnO_x nanoclusters by lowering the preparation temperature of the catalyst down to 85 K, a significant enhancement of $^{13}CO_2$ activation was observed. Such an activation phenomenon likely takes place via the formation of relatively strongly bound intermediates with a prominent role of the interfacial sites, involving both MnO_x and adjacent Pd atoms. The interfacial character of the active sites well correlates with the observation of maximum $^{13}CO_2$ activation at less than a monolayer of MnO_x coverage, while complete wetting of the Pd(111) surface with MnO_x blocks the metal sites and inhibits $^{13}CO_2$ activation.

Future development of a truly efficient catalyst for CO_2 conversion into different, value-added products will require a comprehensive atomistic knowledge of the adsorption and activation mechanisms involved. Initiation of the activation is the first critical step. The hydrogenation of the intermediates on the MnO_x/Pd(111) model system will be the subject of our forthcoming studies.

Experimental Section

The experiments were conducted in a custom-made ultra-high vacuum (UHV) chamber with a base pressure of 7×10^{-11} Torr that has been described in detail previously.[70] The Pd(111) single crystal (MaTeck GmbH, 10 mm diameter × 1 mm thick disk, 99.999% purity) was cleaned by several cycles of Ar^+ (Ar(g), Linde GmbH, Purity 99.999%) sputtering (LK technologies, NGI3000, 1.5 kV × 15 mA) followed by annealing at 1000 K. Pd(111) surface cleanness was verified by both XPS (Riber non-monochromatized Al Kα x-ray excitation, 300 W, Riber EA150 electron energy analyzer) and TPD, where in the latter case CO/CO_2 (due to surface contamination) was monitored upon O_2 (O_2(g) LindeGmbH, Purity 99.999%) adsorption on the clean Pd(111) surface.[31] The model catalytic system was prepared in situ by evaporating ultra-thin Mn overlayers from a Mn metal source (Mn foil casted, 1 mm × 5 mm in dimensions, MaTeck GmbH, > 99.9% purity) on the clean Pd(111) surface either at 85 K or at RT. In both cases, XPS has revealed the presence of metallic (Mn^0) and several oxidic (Mn^{2+} and Mn^{3+}) states. The partial oxidation of Mn is tentatively attributed to the reaction of Mn with water/hydroxide species generated due to the background pressure spike occurring during the Mn deposition. The coverage of the MnO_x (Θ_{MnOx}) overlayers on Pd(111) substrate was calibrated using XPS. This is accomplished by monitoring the break point in the

linear dependence of Pd 3d intensity as a function of the Mn deposition time at RT.[54] As shown in Figure S6c, such an analysis revealed a 'quasi' Stranski-Krastanov cluster growth mode at RT.[54] In contrast, corresponding data for the Mn deposition at 85 K closely fits an exponential, break-free decay, as expected for self-affine growth,[46–47] (and therefore, the calibration for 85 K utilized that of RT). In the TPD measurements, a quadrupole mass spectrometer (QMS, Ametek Dycor Dymaxion DM200) with an apertured shield and a proportional–integral–derivative (PID) controlled sample heater (Heatwave, model 101303) were employed. TPD experiments were carried out using a heating rate of 1 K/s, a 70 eV QMS electron ionization energy, and a 30 ms dwell time for each desorption channel. After each TPD experiment, model catalyst surface was cleaned via Ar^+ sputtering and a fresh model catalyst surface was prepared due to the thermally induced sintering and chemical modification of the small MnO_x clusters during the TPD runs. $^{13}CO_2$ (Cambridge Isotopes, purity 99.8%) or D_2 (Cambridge Isotopes, purity 99.9%) were admitted into the chamber via a dedicated tube doser. The exposures, ε, are presented in Langmuir units (1 L = 10^{-6} Torr·s), while taking into account an enhancement factor (~7) of the doser in comparison with an isotropic dosing by chamber backfilling.

Supporting Information Summary

Supporting Information presents $^{13}CO_2$ and D_2 TPD profiles and Pd 3d XPS spectra for different MnO_x overlayer coverages, $^{13}CO_2$ TPD from the clean Pd(111) surface, whereas additional references are cited within the Supporting Information.[71–73]

Acknowledgements

I. L. and E. O. acknowledge The Scientific and Technological Research Council of Turkey (TUBITAK) and Horizon 2020 Marie Sklodowska-Curie CoCirculation2 Program (Grant No: 119C014).

Conflict of Interests

The authors declare no conflict of interest.

Data Availability Statement

The data that support the findings of this study are available from the corresponding author upon reasonable request.

Keywords: carbon dioxide activation · manganese oxides · Pd · nanomaterials · clusters

[1] M. Aresta, A. Dibenedetto, A. Angelini, *Chem. Rev.* **2014**, *114*, 1709–1742.
[2] A. M. Appel, J. E. Bercaw, A. B. Bocarsly, H. Dobbek, D. L. DuBois, M. Dupuis, J. G. Ferry, E. Fujita, R. Hille, P. J. A. Kenis, C. A. Kerfeld, R. H. Morris, C. H. F. Peden, A. R. Portis, S. W. Ragsdale, T. B. Rauchfuss, J. N. H. Reek, L. C. Seefeldt, R. K. Thauer, G. L. Waldrop, *Chem. Rev.* **2013**, *113*, 6621–6658.
[3] Y. Li, S. H. Chan, Q. Sun, *Nanoscale* **2015**, *7*, 8663–8683.
[4] S. Saeidi, N. A. S. Amin, M. R. Rahimpour, *J. CO_2 Util.* **2014**, *5*, 66–81.
[5] B. Hu, C. Guild, S. L. Suib, *J. CO_2 Util.* **2013**, *1*, 18–27.
[6] M. Aresta, *Carbon Dioxide as Chemical Feedstock*, WileyVCH, New York, **2010**.
[7] S. Kattel, P. Liu, J. G. Chen, *J. Am. Chem. Soc.* **2017**, *139*, 9739–9754.
[8] J. A. Rodriguez, P. Liu, D. J. Stacchiola, S. D. Senanayake, M. G. White, J. G. Chen, *ACS Catal.* **2015**, *5*, 6696–6706.
[9] M. Behrens, F. Studt, I. Kasatkin, S. Kühl, M. Hävecker, F. Abild-Pedersen, S. Zander, F. Girgsdies, P. Kurr, B.-L. Kniep, M. Tovar, R. W. Fischer, J. K. Nørskov, R. Schlögl, *Science* **2012**, *336*, 893–897.
[10] E. V. Kondratenko, G. Mul, J. Baltrusaitis, G. O. Larrazábal, J. Pérez-Ramírez, *J. Energy Environ. Sci.* **2013**, *6*, 3112–3135.
[11] E. A. Quadrelli, G. Centi, J.-L. Duplan, S. Perathoner, *ChemSusChem* **2011**, *4*, 1194–1215.
[12] A. Álvarez, M. Borges, J. J. Corral-Pérez, J. G. Olcina, L. Hu, D. Cornu, R. Huang, D. Stoian, A. Urakawa, *ChemPhysChem* **2017**, *18*, 3135–3141.
[13] T. Hyakutake, W. van Beek, A. Urakawa, *J. Mater. Chem. A* **2016**, *4*, 6878–6885.
[14] D. B. Clarke, I. Suzuki, A. T. Bell, *J. Catal.* **1993**, *142*, 27–36.
[15] I. A. Fisher, A. T. Bell, *J. Catal.* **1996**, *162*, 54–65.
[16] A. Baiker, *Appl. Organomet. Chem.* **2000**, *14*, 751–762.
[17] Y. Yang, J. Evans, J. A. Rodriguez, M. G. White, P. Liu, *Phys. Chem. Chem. Phys.* **2010**, *12*, 9909–9917.
[18] M. Bowker, R. A. Hadden, H. Houghton, J. N. K. Hyland, K. C. Waugh, *J. Catal.* **1988**, *109*, 263–273.
[19] A. A. Gokhale, J. A. Dumesic, M. Mavrikakis, *J. Am. Chem. Soc.* **2008**, *130*, 1402–1414.
[20] T. E. James, S. L. Hemmingson, C. T. Campbell, *ACS Catal.* **2015**, *5*, 5673–5678.
[21] J. Schumann, M. Eichelbaum, T. Lunkenbein, N. Thomas, M. C. Álvarez Galván, R. Schlögl, M. Behrens, *ACS Catal.* **2015**, *5*, 3260–3270.
[22] D. J. Stacchiola, S. D. Senanayake, P. Liu, J. A. Rodriguez, *Chem. Rev.* **2013**, *113*, 4373–4390.
[23] M. Misono, in *Heterogeneous Catalysis of Mixed Oxides*, Elsevier, New York, **2013**.
[24] A. B. Boffa, A. T. Bell, G. A. Somorjai, *J. Catal.* **1993**, *139*, 602–610.
[25] F. Li, G. Parteder, F. Allegretti, C. Franchini, R. Podloucky, S. Surnev, F. P. Netzer, *J. Phys. Condens. Matter* **2009**, *21*, 134008.
[26] B. Yoon, H. Häkkinen, U. Landman, A. S. Wörz, J.-M. Antonietti, S. Abbet, K. Judai, U. Heiz, *Science* **2005**, *307*, 403–407.
[27] C. T. Campbell, *Nat. Chem.* **2012**, *4*, 597–598.
[28] J. C. Matsubu, V. N. Yang, P. Christopher, *J. Am. Chem. Soc.* **2015**, *137*, 3076–3084.
[29] F. Solymosi, A. Erdöhelyi, M. Lancz, *J. Catal.* **1985**, *95*, 567–577.
[30] T. Matsushima, *J. Phys. Chem.* **1987**, *91*, 6192–6197.
[31] H. Conrad, G. Ertl, E. E. Latta, *Surf. Sci.* **1974**, *41*, 435–446.
[32] G. E. Gdowski, T. E. Felter, R. H. Stulen, *Surf. Sci.* **1987**, *181*, L147-L155.
[33] F. R. Lucci, M. T. Darby, M. F. G. Mattera, C. J. Ivimey, A. J. Therrien, A. Michaelides, M. Stamatakis, E. C. H. Sykes, *J. Phys. Chem. Lett.* **2016**, *7*, 480–485.
[34] T. Mitsui, M. K. Rose, E. Fomin, D. F. Ogletree, M. Salmeron, *Nature* **2003**, *422*, 705–707.
[35] Z. He, M. Cui, Q. Qian, J. Zhang, H. Liu, B. Han, *Proc. Nat. Acad. Sci.* **2019**, *116*, 12654.
[36] A. Dubey, L. Nencini, R. R. Fayzullin, C. Nervi, J. R. Khusnutdinova, *ACS Catal.* **2017**, *7*, 3864–3868.
[37] B. R. Landoldt, in *Numerical Data and Functional Relationships in Science and Technology*, Springer, Berlin, **1997**.
[38] W. Taifan, J.-F. Boily, J. Baltrusaitis, *Surf. Sci. Rep.* **2016**, *71*, 595–671.
[39] H. J. Freund, M. W. Roberts, *Surf. Sci. Rep.* **1996**, *25*, 225–273.
[40] X.-F. Yang, A. Wang, B. Qiao, J. Li, J. Liu, T. Zhang, *Acc. Chem. Res.* **2013**, *46*, 1740–1748.
[41] G. A. Somorjai, J. Y. Park, *Chem. Soc. Rev.* **2008**, *37*, 2155–2162.
[42] A. A. Herzing, C. J. Kiely, A. F. Carley, P. Landon, G. J. Hutchings, *Science* **2008**, *321*, 1331–1335.
[43] Y. Lei, F. Mehmood, S. Lee, J. Greeley, B. Lee, S. Seifert, R. E. Winans, J. W. Elam, R. J. Meyer, P. C. Redfern, D. Teschner, R. Schlögl, M. J. Pellin, L. A. Curtiss, S. Vajda, *Science* **2010**, *328*, 224–228.
[44] M. Turner, V. B. Golovko, O. P. H. Vaughan, P. Abdulkin, A. Berenguer-Murcia, M. S. Tikhov, B. F. G. Johnson, R. M. Lambert, *Nature* **2008**, *454*, 981–983.
[45] W. E. Kaden, T. Wu, W. A. Kunkel, S. L. Anderson, *Science* **2009**, *326*, 826–829.
[46] J. A. Thornton, *Annu. Rev. Mater. Sci.* **1977**, *7*, 239–260.

[47] J. A. Venables, G. D. T. Spiller, M. Hanbucken, *Rep. Prog. Phys.* **1984**, *47*, 399–459.
[48] V. F. Kiselev, O. V. Krylov, in *Adsorption and Catalysis on Transition Metals and Their Oxides*, Springer-Verlag Berlin Heidelberg, **1989**.
[49] S. Natesakhawat, P. R. Ohodnicki, B. Howard, J. Lekse, J. Baltrus, C. Matranga, *Top. Catal.* **2013**, *56*.
[50] L. G. Tejuca, A. T. Bell, V. Cortés Corberán, *Appl. Surf. Sci.* **1989**, *37*, 353–366.
[51] I. A. Bönicke, W. Kirstein, F. Thieme, *Surf. Sci.* **1994**, *307–309*, 177–181.
[52] G. C. Chinchen, M. S. Spencer, K. C. Waugh, D. A. Whan, *J. Chem. Soc. Faraday Trans. 1* **1987**, *83*, 2193–2212.
[53] N. Schumacher, K. Andersson, L. C. Grabow, M. Mavrikakis, J. Nerlov, I. Chorkendorff, *Surf. Sci.* **2008**, *602*, 702–711.
[54] B. Karakurt, Y. Kocak, I. Lyubinetsky, E. Ozensoy, *J. Phys. Chem. C* **2020**, *124*, 22529–22538.
[55] A. Sandell, A. J. Jaworowski, *J. Electron Spectrosc. Relat. Phenom.* **2004**, *135*, 7–14.
[56] O. Rader, E. Vescovo, M. Wuttig, D. D. Sarma, S. Blügel, F. J. Himpsel, A. Kimura, K. S. An, T. Mizokawa, A. Fujimori, C. Carbone, *Europhys. Lett.* **1997**, *39*, 429–434.
[57] O. Rader, T. Mizokawa, A. Fujimori, A. Kimura, *Phys. Rev. B* **2001**, *64*, 165414.
[58] P. Schieffer, C. Krembel, M. C. Hanf, G. Gewinner, *J. Electron Spectrosc. Relat. Phenom.* **1999**, *104*, 127–134.
[59] B. R. Strohmeier, D. M. Hercules, *J. Phys. Chem.* **1984**, *88*, 4922–4929.
[60] A. Aoki, *Jpn. J. Appl. Phys.* **1976**, *15*, 305–311.
[61] M. C. Biesinger, B. P. Payne, A. P. Grosvenor, L. W. M. Lau, A. R. Gerson, R. S. C. Smart, *Appl. Surf. Sci.* **2011**, *257*, 2717–2730.
[62] M. Oku, K. Hirokawa, S. Ikeda, *J. Electron Spectrosc. Relat. Phenom.* **1975**, *7*.
[63] V. Di Castro, G. Polzonetti, *J. Electron Spectrosc. Relat. Phenom.* **1989**, *48*, 117–123.
[64] J. S. Foord, R. B. Jackman, G. C. Allen, *Philos. Mag. A* **1984**, *49*, 657–663.
[65] M. Bowker, *ChemCatChem* **2019**, *11*, 4238–4246.
[66] J. Y. Park, L. R. Baker, G. A. Somorjai, *Chem. Rev.* **2015**, *115*, 2781–2817.
[67] P. C. Stair, *Nat. Chem.* **2011**, *3*, 345–346.
[68] A. Sandell, P. H. Andersson, E. Holmström, A. J. Jaworowski, L. Nordström, *Phys. Rev. B* **2001**, *65*, 035410.
[69] M. Cargnello, V. V. T. Doan-Nguyen, T. R. Gordon, R. E. Diaz, E. A. Stach, R. J. Gorte, P. Fornasiero, C. B. Murray, *Science* **2013**, *341*, 771–773.
[70] B. Karakurt, Y. Kocak, E. Ozensoy, *J. Phys. Chem. C* **2019**, *123*, 28777–28788.
[71] P. K. Schmidt, K. Christmann, G. Kresse, J. Hafner, M. Lischka, A. Groß, *Phys. Rev. Lett.* **2001**, *87*, 096103.
[72] C. Amorim, M. A. Keane, *J. Colloid Interface Sci.* **2008**, *322*, 196–208.
[73] A. Tamtögl, M. Kratzer, J. Killman, A. Winkler, *J. Chem. Phys.* **2008**, *129*, 224706.

Manuscript received: October 20, 2022
Revised manuscript received: April 21, 2023
Accepted manuscript online: April 27, 2023
Version of record online: ■■, ■■

RESEARCH ARTICLE

Smaller is better: Decreasing the size of the MnO_x nanoclusters on Pd(111) surface leads to a significant enhancement of CO_2 activation.

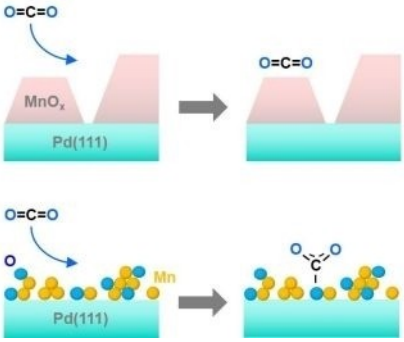

A. Anil, O. F. Sadak, B. Karakurt, Dr. Y. Kocak, Dr. I. Lyubinetsky, Prof. Dr. E. Ozensoy**